EPR/ENDOR, Mössbauer, and Quantum Chemical Investigation of Di-iron Complexes Mimicking the Active Oxidized State of [FeFe] Hydrogenase.

Alexey Silakov[#*†], Matthew T. Olsen[+], Stephen Sproules[#§], Eduard J. Reijerse[#],

Thomas B. Rauchfuss[+], Wolfgang Lubitz[#*]

[#] Max-Planck-Institut für Chemische Energiekonversion, Stiftstr. 34-36, Mülheim a.d. Ruhr, 45470, Germany

[§] School of Chemistry and Photon Science Institute, The University of Manchester, Oxford Road, Manchester M13 9PL, U.K.

[+] Department of Chemistry, University of Illinois, A328 Chemical & Life Sciences Lab, 600 South Mathews Avenue, Urbana, IL 61801, USA

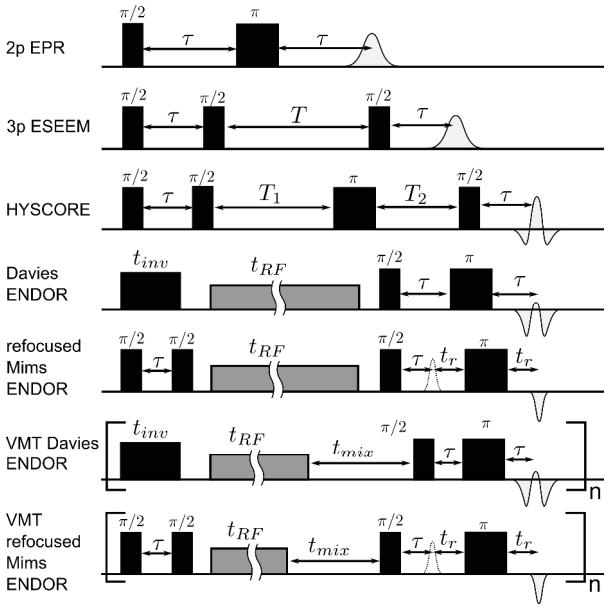

Figure S1. Pulse EPR sequences used in this study.

In the VMT ENDOR technique the delay time between the RF pulse and the detection sequence (t_{mix}) is increased (see Figure S1), which skews the profile of the ENDOR doublet due to a difference in nuclear and electronic T_1 relaxation rates. In some cases a complete polarization of the ENDOR signal can be observed. VMT ENDOR experiments can be performed using both Mims and Davies experiments. The effect is best observed at low temperatures and high MW frequencies, as it is governed by the Boltzmann polarization factor $\varepsilon = hv/kT$. The "VMT effect" can also be enhanced by using linear scanning instead of stochastic data acquisition with n more than10 shots per point [1], although this enhancement comes at the cost of increasing

baseline artifacts. To observe the VMT effect slow electron-nuclear cross-relaxation (T_x) and nuclear spin-lattice relaxations (T_{1n}) with respect to the longitudinal electron relaxation times (T_{1e}) are required. For the current system $T_{1e} \approx 50$ µs at 25K is estimated. As the anisotropy of the observed $^{31}P(PMe_3)$ HF coupling is rather small (see Table 1), we expect very slow cross-relaxation i.e. $T_x >> T_{1e}$. Indeed, even at this relatively high temperature (25K), we have observed an almost completely polarized ^{31}P Q-band ENDOR spectrum when t_{mix} is above 100 µs (see Figure 4 in the main text).

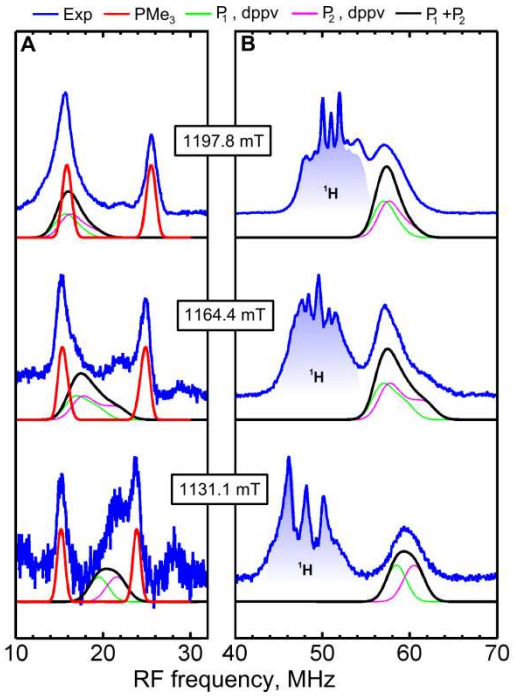

Figure S2. Q-band Davies ENDOR spectra (blue) of **1edt** for two different RF regions (**A**, **B**) measured at the indicated field positions in the EPR spectrum at T = 20K. Simulations were performed using parameters from Table 1 (see legend above the graph). The ^1H ENDOR region is shaded blue for clarity. Experimental conditions: **A**, t_{RF} = 35 µs; ν_{mw} = 33.8708 GHz; t_{inv} = 200ns. **B**, t_{RF} = 5.5 µs; ν_{mw} = 33.8708 GHz; t_{inv} = 80 ns.

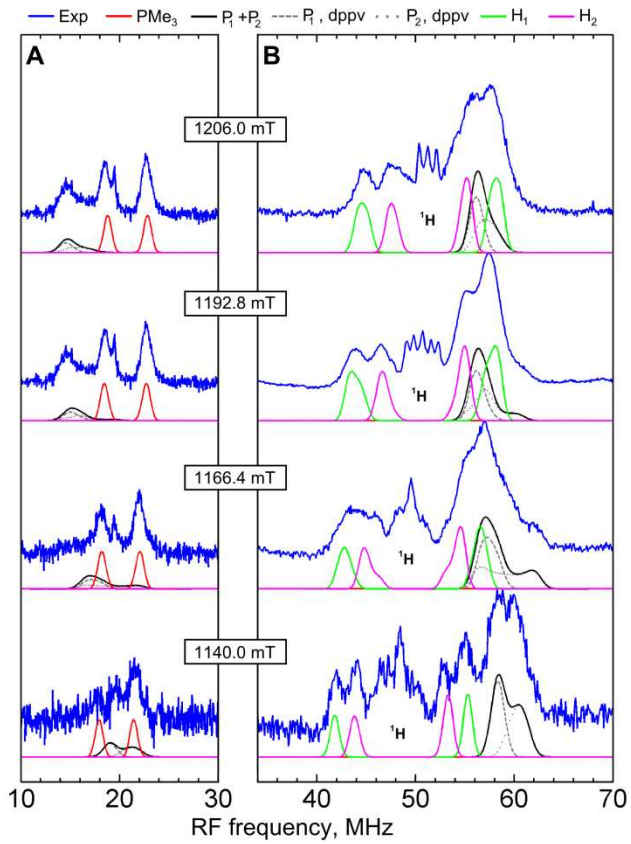

Figure S3. Q-band ENDOR spectra of **1adt** measured at the indicated field positions at 20 K. Low frequency spectra (**A**) were recorded using the refocused Mims ENDOR sequence with τ = 108 ns and t(π/2) = 16 ns, whereas the high frequency part (**B**) was recorded using Davies ENDOR, t_{inv} = 44 ns (suppressing matrix ^{1}H signals), t(π/2) = 16 ns, τ = 400 ns. Simulations were performed using the HF coupling constants listed in Table 1 (see legend above the graph for the color coding).

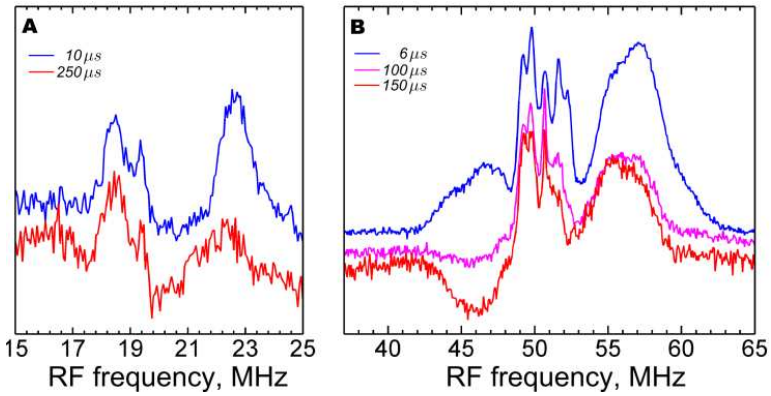

FigureS4. Q-band variable mixing time (VMT) ENDOR measurements of **1adt** at the field position of maximum echo intensity (1192.0 mT) showing the effect of t_{mix} on the spectral profile. All spectra are normalized to the most prominent unchanged feature. Experimental conditions: **A**, refocused Mims ENDOR, T = 20 K; t_{RF} = 45 μs; ν_{mw} = 33.8761 GHz; B_0 = 1192.0 mT; τ = 108 ns, SRT = 550 μs. **B**, Davies ENDOR, T = 25 K; t_{RF} = 6 μs; ν_{mw} = 33.8250 GHz; B_0 = 1191.3 mT; t_{inv} = 80 ns; SRT = 550 μs.

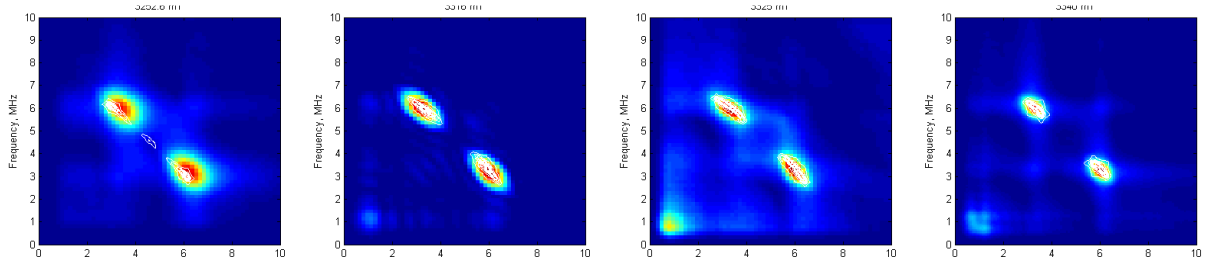

Figure S5. W-band HYSCORE spectra measured at various field positions. Overlaying white contours are the simulations accounting for one ^{57}Fe HF coupling (Fe_2, see Table 1).

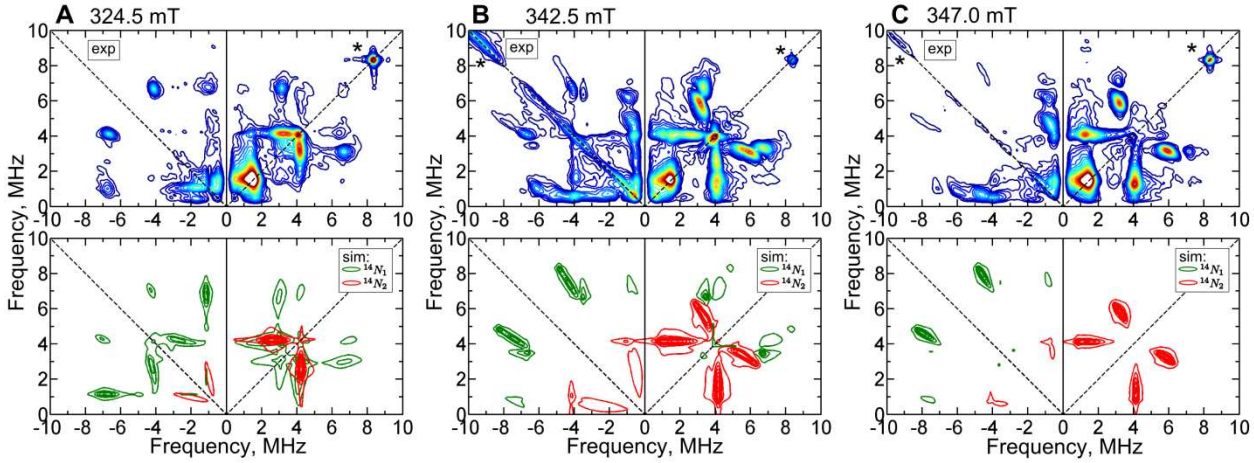

Figure S6. X-band HYSCORE spectra of **1adt** (top), measured at the indicated field positions and corresponding simulations (bottom) accounting for two independent ^{14}N signals that correspond to two isomeric forms of the amine group. Experimental parameters: T = 20 K; ν_{mw} = 9.720 GHz; $t(\pi/2)$ = 8 ns; τ = 86 ns. For clarity the presented spectra are cropped to the low frequency range, neglecting the ^{1}H signals. Asterisks denote instrumental artifacts. Simulations include ^{31}P(dppv) HF coupling constants in the orientation selection calculation.

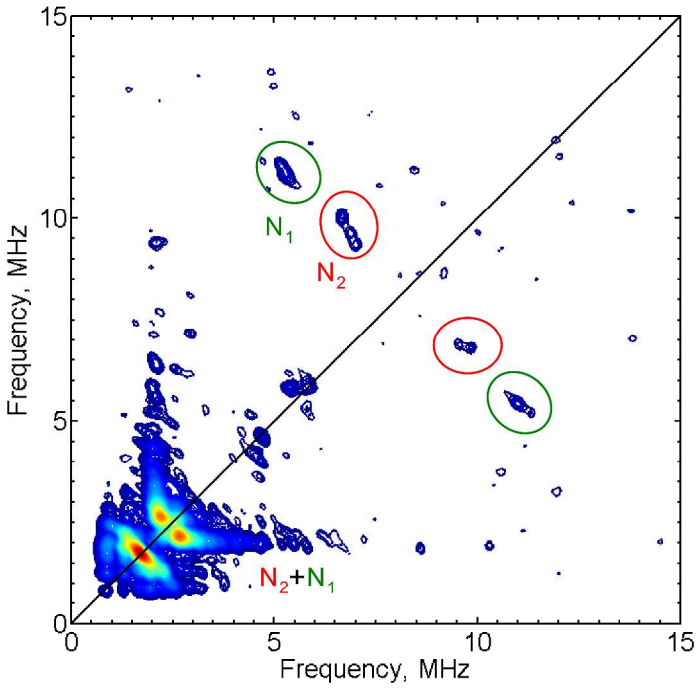

Figure S7. Q-band HYSCORE spectrum of non-enriched **1adt** recorded at T = 25K. Experimental parameters: B_0 = 1160 mT; ν_{mw} = 9.720 GHz; t(π/2) = 12ns; τ = 300 ns. Green and red circles indicate positions of double quantum transitions for N_1 and N_2 nuclei respectively.

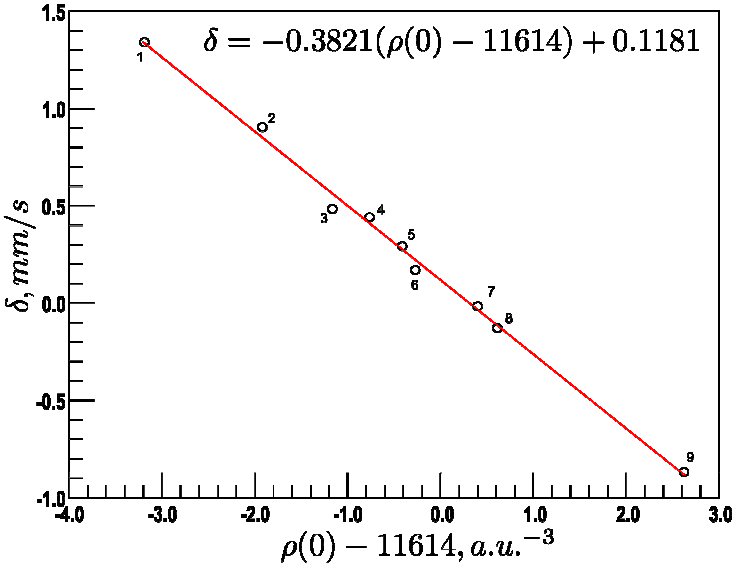

Figure S8. Correlation between experimentally measured isomeric shifts (δ) for various iron model complexes (see Table S1) and DFT calculated electron densities at the iron nucleus $\rho(0)$. A constant 11614 a.u.$^{-3}$ is subtracted from $\rho(0)$ for convenience. Correlation between δ and $\rho(0)$ is approximated by a linear function, as denoted on the top of the plot.

Table S1. Electron densities at the nucleus ρ(0) and experimental isomer shifts δ^{exp} for all investigated complexes calculated using the unrestricted B3LYP functional in concert with Wachters basis set on the irons and TZVPP on all other atoms. Geometries and experimental values for all but [Fe(I) diketiminate] were taken from the work by Römelt.[2] Experimental isomer shift value and starting crystallographic data for [Fe(I) diketiminate] were taken from the work of Stoian,[3] prior to the calculation of Mössbauer parameters, the geometry was optimized on the BP86/TZVPP level.

N	Name	S	δ^{exp}, mm/s	ρ(0), a.u.$^{-3}$
1	$Fe(II)F_6^{4-}$	2	1.34	11610.8
2	$Fe(II)Cl_4^{2-}$	2	0.90	11612.1
3	$Fe(III)F_6^{3-}$	5/2	0.48	11612.8
4	Fe(I) Diketiminate	3/2	0.44	11613.2
5	$[Fe(III)Az]^{+}$	1/2	0.29	11613.6
6	$Fe(IV)TMCO^{2+}$	1	0.17	11613.7
7	$Fe(II)CN_6^{4-}$	0	-0.02	11614.4
8	$Fe(III)CN_6^{3-}$	1/2	-0.13	11614.6
9	$Fe(IV)O_4^{2-}$	1	-0.87	11616.6

Table S2. Short description of the basis sets used for figure 12 and figure S8 including contraction patterns where applicable.

Abbreviated BS names	Description
SVP	Ahlrichs split valence basis set with one set of first polarization functions on all atoms including hydrogen[4]. Fe: 5s3p2d pattern {63311/531/41}
dec-SVP	Decontracted SVP [4] Fe: 14s9p5d
TZVPP	Ahlrichs triple-ζ valence basis set with three sets of first polarization functions on all atoms including hydrogens. [4] Fe: 6s4p3d1f pattern {842111/6311/411/1}
Def2-TZVPP	Balanced basis sets of triple-ζ valence[5] Fe: 6s5p4d2f1g pattern {842111/63111/4111/11/1}
aug-cc-pVTZ	Augmented version of Dunning correlation consistent polarized triple-ζ basis set including diffuse functions. [6] Fe : 7s6p4d2f1g pattern {19 19 19 19 19 19 1/15 15 15 15 15 1/7771/11/1}
Ross-ANO-TZV	Augmented Roos triple-ζ ANO Atomic Natural Orbital Basis Set[7] Fe: 8s7p5d3f2g pattern {2121212121212121/15151515151515/1010101010/666/44}
Bonn-ANO-TZ3P	Atomic Natural Orbital basis set with a contracted set of f-polarization functions on the heavy atoms. Bonn ANO basis sets are based on the gaussian primitives from the TZV basis of A. Schaefer, H. Horn and R. Ahlrichs, J. Chem. Phys. 97, 2571 (1992). [F. Neese, 2007, unpublished] Fe: 7s6p4d3f2g pattern {1919191818191/14141414141/10101010/666/44}
QZVP	Ahlrichs quadruple-ζ basis set. [4] Fe: 11s6p5d3f2g pattern {114111111111/951111/61111/111/11}
Wachters	Wachters basis set[8] Fe: 8s6p4d2f pattern {62111111/331211/3111/21}
CP(PPP)	The ORCA basis set 'CoreProp'. This basis is based on the TurboMole DZ basis developed by Ahlrichs and coworkers and obtained from the basis set library under ftp.chemie.uni-karlsruhe.de/pub/basen Fe: 17s7p3d1f pattern {11111111111111111/3311111/311/1}
Partridge-3	Large uncontracted basis set[9] Fe: 23s16p8d

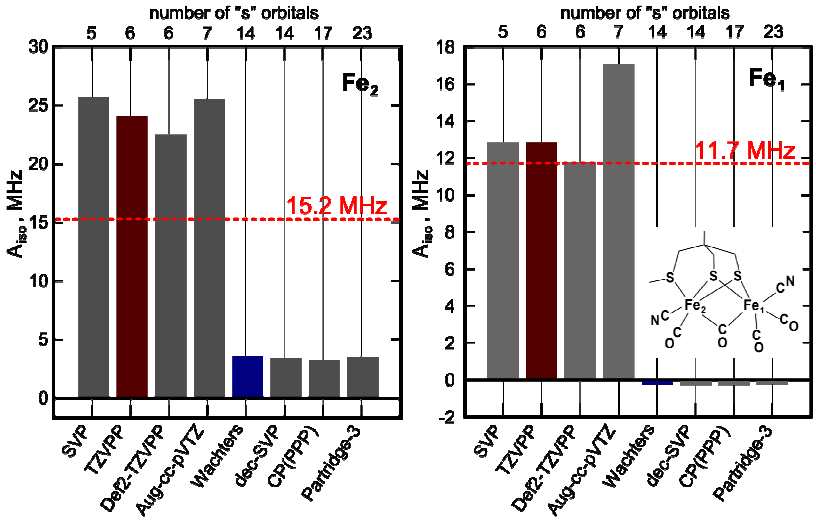

Figure S9. ^{57}Fe A_{iso} coupling constants of {2Fe3S} model compound as calculated using various basis sets for the irons in conjunction with the B3LYP functional and the TZVPP basis set on all the other atoms. The red dashed lines indicate the experimentally obtained values from the work of Silakov et al [10]. Red and blue bars indicate TZVPP and Wachters basis sets respectively to enhance visual representation. In the insert (right) a schematic representation of the model is shown.

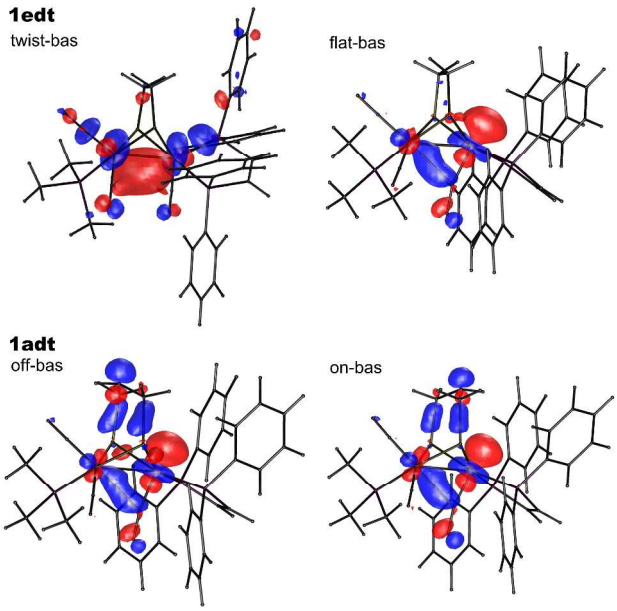

Figure S10. HOMO orbitals of selected isomers of **1edt** and **1adt** obtained from spin unrestricted B3LYP calculations using Wachters basis set for Fe atoms and TZVPP for all other atoms.

Table S3. Comparison of calculated spectroscopic parameters of **1edt** with experimental data.

1edt	twist-ap	twist-bas	flat-ap	flat-bas	exp
Single point energy					
E^{B3LYP}, Eh	-5889.392017	-5889.391960	-5889.397913	-5889.401140	-
ΔE, kcal/mol	5.73	5.76	2.03	0.00	-
g-matrix					
g_x	2.0175	2.0280	2.0143	2.0142	2.009
g_y	2.1320	2.1261	2.0293	2.0320	2.028
g_z	2.1667	2.1666	2.0951	2.0935	2.139
g_{iso}	2.1054	2.1069	2.0462	2.0465	2.059
^{57}Fe, Fe$_1$[a]					
A_{iso} (MHz)	-0.55 (-5.03)	+0.97 (-3.46)	-4.59 (-6.77)	-4.74 (-7.05)	-8.30
A_{dip} (MHz)	+11.14 (+13.38)	+9.64 (+11.71)	+15.97 (+16.91)	+16.58 (+17.53)	+12.45
A_{rh}	+0.57 (+0.68)	+0.99 (+0.79)	+0.46 (+0.61)	+0.35 (+0.46)	+0.70
ΔE_Q (mm/s)[c]	+1.47	-1.17	-0.41	-0.49	-0.58
η	0.87	0.87	0.91	0.97	0.90
ρ(0) (a.u.$^{-3}$)	11613.9141	11613.9519	11613.8685	11613.8898	
δ (mm/s)[b]	+0.15	+0.14	+0.17	+0.16	+0.20
S.p. (Loewdin)	0.7240	0.6643	0.9111	0.9460	
S.p. (Mulliken)	0.7448	0.7023	0.9740	1.0189	
^{57}Fe, Fe$_2$[a]					
A_{iso} (MHz)	-0.57 (-2.65)	+0.55 (-1.48)	-2.25 (-2.39)	-1.99 (-2.08)	-1.60
A_{dip} (MHz)	+5.77 (+6.75)	+7.17 (+7.95)	+2.02 (+2.01)	+1.43 (+1.40)	+1.30
A_{rh}	+0.64 (+0.59)	+0.79 (+0.68)	+0.30 (+0.36)	+0.23 (+0.21)	+0.69
ΔE_Q (mm/s)[c]	+0.70	-0.59	+0.67	+0.80	+0.70
η	0.99	0.69	0.52	0.48	0.92
δ (mm/s)[b]	-0.03	-0.01	+0.01	+0.01	+0.04
S.p. (Loewdin)	0.3711	0.4225	0.1043	0.0747	
S.p. (Mulliken)	0.3946	0.4178	0.1147	0.0797	
^{31}P(dppv)					
A_{iso} (MHz)	-66.85	-60.13	-85.17	-82.29	-77.30
A_{iso} (MHz)	-60.78	-58.69	-84.39	-85.70	-77.30
^{31}P(PMe3)					
A_{iso} (MHz)	+8.15	-40.22	+6.10	-11.91	-9.70

[a] HF tensors are parameterized as such: $A = A_{iso}+A_{dip}[-1+A_{rh}, -1-A_{rh}, 2]$. The values in brackets are obtained excluding second order spin-orbit coupling contribution.

[b] $\delta = 0.1181 - 0.3821\ (\rho(0) - 11614)$, see materials and methods for details.

[c] As the asymmetry parameter is almost 100% the sign of ΔE_Q does not have a physical meaning

Table S4. Comparison of calculated spectroscopic parameters of **1adt** with experimental data. S.p. = spin density. Note that signs of ^{14}N hyperfine coupling constants were not identified experimentally.

1adt	***ap-on***	***bas-on***	***ap-off***	***bas-off***	exp
Single point energy					
E^{B3LYP}, Eh	-5944.726416	-5944.730859	-5944.724231	-5944.73035	
ΔE, kcal/mol	2.79	0.00	4.16	0.32	
g-matrix					
g_x	2.0151	2.0146	2.0128	2.0139	2.005
g_y	2.0323	2.0304	2.0271	2.0293	2.031
g_z	2.0919	2.0933	2.0920	2.0902	2.125
g_{iso}	2.0464	2.0461	2.0440	2.0444	2.054
^{57}Fe, Fe$_1$[a)]					
A_{iso} (MHz)	-6.22 (-8.38)	-6.33 (-8.69)	-6.99 (-9.13)	-7.44 (-9.66)	
A_{dip} (MHz)	+15.10 (+16.01)	+16.04 (+17.00)	+14.42 (+15.69)	+14.93 (+15.85)	
A_{rh}	+0.74 (+0.87)	+0.50 (+0.64)	+0.89 (+0.96)	+0.81 (+0.94)	
ΔE_Q (mm/s)	+0.34	+0.39	-0.39	-0.38	
η	0.53	0.13	0.76	0.68	
ρ(0) (a.u.$^{-3}$)	11613.8189	11613.7785	11613.8156	11613.8349	
δ (mm/s)[b)]	+0.19	+0.20	+0.19	+0.18	
S.p. (Loewdin)	0.9003	0.9579	0.9356	0.9613	
S.p. (Mulliken)	0.9772	1.0327	0.9959	1.0248	
^{57}Fe, Fe$_2$[a)]					
A_{iso} (MHz)	-1.65 (-1.84)	-1.79 (-1.84)	-1.76 (-1.79)	-1.36 (-1.39)	
A_{dip} (MHz)	+1.76 (+1.79)	+1.21 (+1.12)	+1.41 (+1.34)	+0.82 (+0.70)	
A_{rh}	+0.63 (+0.75)	+0.15 (+0.23)	+0.57 (+0.81)	+0.29 (+0.66)	
ΔE_Q (mm/s)	+0.83	+0.94	+0.73	+0.89	
η	0.40	0.53	0.63	0.59	
ρ(0) (a.u.$^{-3}$)	11614.2319	11614.2360	11614.2242	11614.2519	
δ (mm/s)[b)]	+0.03	+0.03	+0.03	+0.02	
S.p. (Loewdin)	0.0910	0.0577	0.0584	0.0293	
S.p. (Mulliken)	0.1058	0.0650	0.0695	0.0412	
^{14}N(adt)					
A_{iso} (MHz)	+3.92	+2.91	+0.59	+0.83	+4.00 | +1.17
A_{dip} (MHz)	+0.21	+0.22	+0.66	+0.72	+0.68 | +1.17
A_{rh}	+0.34	+0.24	+0.03	+0.03	+0.51 | +0.0
K (MHz)	-1.24	-1.25	-1.24	-1.22	1.12 | 1.15
η	0.09	0.07	0.07	0.11	0.20 | 0.0
^{31}P(dppv)					
P_1, A_{iso} (MHz)	-88.27	-83.85	-86.23	-82.08	-73.0
P_2, A_{iso} (MHz)	-92.01	-88.30	-86.22	-87.38	-75.3
^{31}P(PMe$_3$)					
P_3, A_{iso} (MHz)	+8.39	-9.61	+9.59	-6.67	-3.90
^{1}H(ADT)[c)]					
H_1, A_{iso} (MHz)	+2.68	+1.37	+7.05	+4.95	+8.30
H_2, A_{iso} (MHz)	+1.95	+1.78	+7.07	+7.67	+13.50
H_3, A_{iso} (MHz)	-1.30	-0.81	-0.87	-1.19	-
H_4, A_{iso} (MHz)	-1.32	-0.77	-1.07	-1.00	-
^{1}H(NH)					
A_{iso}, (MHz)	-0.60	-0.41	-1.07	-0.92	-

[a)] HF tensors are parameterized as such: $A = A_{iso}+A_{dip}[-1+A_{rh}, -1-A_{rh}, 2]$. The values in brackets are obtained excluding second order spin-orbit coupling contribution.

[b)] $\delta = 0.1181 - 0.3821\ (\rho(0) - 11614)$, see materials and methods for details.

c) For assignment of ^{1}H HFCs see Figure S11.

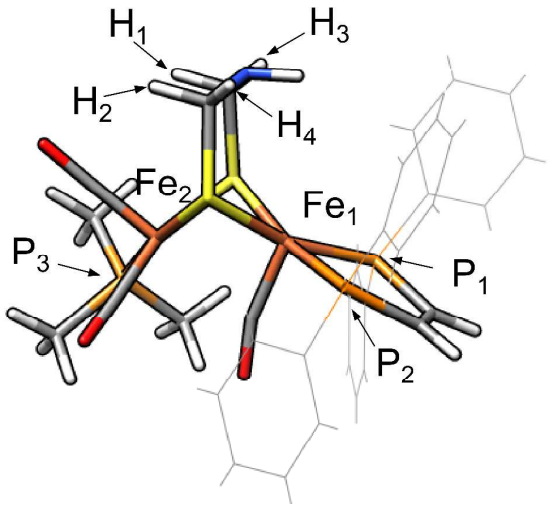

Figure S11. Nomenclature used in tables S3, S4 and tables 4,5 in the main text using ***bas-on 1adt*** geometry as an example.

References

1. Doan, P. E. Combining steady-state and dynamic methods for determining absolute signs of hyperfine interactions: Pulsed ENDOR Saturation and Recovery (PESTRE). *Journal of Magnetic Resonance* **2011,** *208* (1), 76-86.

2. Römelt, M.; Ye, S.; Neese, F. Calibration of modern density functional theory methods for the prediction of 57Fe Mössbauer isomer shifts: meta-GGA and double-hybrid functionals. *Inorg. Chem* **2009,** *48* (3), 784-785.

3. Stoian, S. A.; Yu, Y.; Smith, J. M.; Holland, P. L.; Bominaar, E. L.; Münck, E. Mössbauer, Electron Paramagnetic Resonance, and Crystallographic Characterization of a High-Spin Fe(I) Diketiminate Complex with Orbital Degeneracy. *Inorg. Chem.* **2005,** *44* (14), 4915-4922.

4. Schäfer, A.; Horn, H.; Ahlrichs, R. Fully Optimized Contracted Gaussian-Basis Sets for Atoms Li to Kr. *Journal of Chemical Physics* **1992,** *97* (4), 2571-2577.

5. Weigend, F.; Ahlrichs, R. Balanced basis sets of split valence, triple zeta valence and quadruple zeta valence quality for H to Rn: Design and assessment of accuracy. *Phys. Chem. Chem. Phys.* **2005,** *7* (18), 3297-3305.

6. Balabanov, N. B.; Peterson, K. A. Systematically convergent basis sets for transition metals. I. All-electron correlation consistent basis sets for the 3d elements Sc--Zn. *The Journal of Chemical Physics* **2005,** *123* (6), 064107-064115.

7. Roos, B. O.; Lindh, R.; Malmqvist, P.-A.; Veryazov, V.; Widmark, P. O. New Relativistic ANO Basis Sets for Transition Metal Atoms. *J. Phys. Chem. A* **2005,** *109* (29), 6575-6579.

8. Wachters, A. J. Gaussian Basis Set for Molecular Wavefunctions Containing Third-Row Atoms. *Journal of Chemical Physics* **1970,** *52* (3), 1033

9. Partridge, H. Near Hartree-Fock quality GTO basis sets for the first- and third-row atoms. *The Journal of Chemical Physics* **1989,** *90* (2), 1043-1047.

10. Silakov, A.; Shaw, J. L.; Reijerse, E. J.; Lubitz, W. Advanced Electron Paramagnetic Resonance and Density Functional Theory Study of a {2Fe3S} Cluster Mimicking the Active Site of [FeFe] Hydrogenase. *J Am Chem Soc* **2010**.